J|A|C|S ARTICLES

Published on Web 05/15/2009

Comparative PCET Study of a Donor−Acceptor Pair Linked by Ionized and Nonionized Asymmetric Hydrogen-Bonded Interfaces

Elizabeth R. Young, Joel Rosenthal, Justin M. Hodgkiss, and Daniel G. Nocera*

Department of Chemistry, 6-335, Massachusetts Institute of Technology, 77 Massachusetts Avenue, Cambridge, Massachusetts 02139-4307

Received December 15, 2008; E-mail: nocera@mit.edu

Abstract: A Zn(II) amidinium porphyrin is the excited-state electron donor (D) to a naphthalene diimide acceptor (A) appended with either a carboxylate or sulfonate functionality. The two-point hydrogen bond (···[H$^+$]···) formed between the amidinium and carboxylate or sulfonate functionalities establishes a proton-coupled electron transfer (PCET) pathway for charge transfer. The two D···[H$^+$]···A assemblies differ only by the proton configuration within the hydrogen-bonding interface. Specifically, the amidinium ion transfers a proton to the carboxylate to form a nonionized amidine−carboxylic acid two-point hydrogen network, whereas the amidinium retains both protons when bound to the sulfonate functionality, forming an ionized amidinium−sulfonate two-point hydrogen bond network. These two interface configurations within the dyads thus allow for a direct comparison of the PCET kinetics for the same donor and acceptor juxtaposed by ionized and nonionized hydrogen-bonded interfaces. Analysis of the PCET kinetics ascertained from transient absorption and transient emission spectroscopy reveals that the ionized interface is more strongly impacted by the local solvent environment, thus establishing that the initial static configuration of the proton interface is a critical determinant in the kinetics of PCET.

Introduction

Proton-coupled electron transfer (PCET) networks can be established by using an amidine and a carboxylic acid to juxtapose a donor (D) to an acceptor (A). Unlike symmetric interfaces[1,2] or those that cannot support proton transfer,[3,4] the asymmetric nature of the amidine−carboxylic acid interface underscores the importance of the proton configuration to PCET[5−9] by adding a dipole component to the proton interface.[10,11] Proton fluctuations within the hydrogen-bonding interface couple to the charge shift accompanying the electron transfer through the polarization of the surrounding environment.[12−22] Even in the absence of proton transfer, fluctuations in the proton position within the interface profoundly influence the kinetics of the electron-transfer component of PCET.[9,23] An especially important issue in biology is the effect of ionization on charge-transport rates. Electron transfer may be dramatically altered by the direction of the transferring electron with regard to the orientation of electrostatic and polar fields within the biological milieu.[24−27] In addition, amino acid radical transport rates and yields depend on the ionization state of the amino acid.[28−30] To date, the effect of ionization on PCET has not

(1) Turró, C.; Chang, C. K.; Leroi, G. E.; Cukier, R. I.; Nocera, D. G. *J. Am. Chem. Soc.* **1992**, *114*, 4013–4015.
(2) de Rege, P. J. F.; Williams, S. A.; Therien, M. J. *Science* **1995**, *269*, 1409–1413.
(3) Sessler, J. L.; Wang, B.; Springs, S. L.; Brown, C. T. In *Comprehensive Supramolecular Chemistry*; Murakami, Y., Ed.; Pergamon Press: Oxford, U.K., 1996; Vol. 4, pp 311−336 and references therein.
(4) Chang, C. J.; Brown, J. D.; Chang, M. C. Y.; Baker, E. A.; Nocera, D. G. In *Electron Transfer in Chemistry*; Balzani, V., Ed.; Wiley-VCH: Weinheim, Germany, 2001; Vol. 3.2.4, pp 409−461.
(5) Roberts, J. A.; Kirby, J. P.; Nocera, D. G. *J. Am. Chem. Soc.* **1995**, *117*, 8051–8052.
(6) Roberts, J. A.; Kirby, J. P.; Wall, S. T.; Nocera, D. G. *Inorg. Chim. Acta* **1997**, *263*, 395–405.
(7) Roberts, J. A.; Kirby, J. P.; Nocera, D. G. *J. Am. Chem. Soc.* **1997**, *119*, 9230–9236.
(8) Damrauer, N. H.; Hodgkiss, J. M.; Rosenthal, J.; Nocera, D. G. *J. Phys. Chem. B* **2004**, *108*, 6315–6321.
(9) Hodgkiss, J. M.; Damrauer, N. H.; Pressé, S.; Rosenthal, J.; Nocera, D. G. *J. Phys. Chem. B.* **2006**, *110*, 18853–18858.
(10) Cukier, R. I.; Nocera, D. G. *Annu. Rev. Phys. Chem.* **1998**, *49*, 337–369.
(11) Hodgkiss, J. M.; Rosenthal, J.; Nocera, D. G. In *Hydrogen-Transfer Reactions*; Hynes, J. T., Klinman, J. P., Limbach, H.-H., Schowen, R. L., Eds.; Wiley-VCH: Weinheim, Germany, 2007; Vol. 2.17, pp 503−561.
(12) Cukier, R. I. *J. Phys. Chem.* **1996**, *100*, 15428–15443.
(13) Cukier, R. I. *J. Phys. Chem.* **1994**, *98*, 2377–2381.
(14) Zhao, X. G.; Cukier, R. I. *J. Phys. Chem.* **1995**, *99*, 945–954.
(15) Cukier, R. I. *J. Phys. Chem. A* **1999**, *103*, 5989–5995.
(16) Cukier, R. I. *Biochim. Biophys. Acta* **2004**, *1655*, 37–44.
(17) Hammes-Schiffer, S. In *Electron Transfer in Chemistry*; Balzani, V., Ed.; Wiley-VCH: Weinheim, Germany, 2001; Vol. 1.1.5, p 189.
(18) Hammes-Schiffer, S. *Acc. Chem. Res.* **2001**, *34*, 273–281.
(19) Hammes-Schiffer, S.; Iordanova, N. *Biochim. Biophys. Acta* **2004**, *1655*, 29–36.
(20) Soudackov, A.; Hammes-Schiffer, S. *J. Chem. Phys.* **1999**, *111*, 4672–4687.
(21) Soudackov, A.; Hammes-Schiffer, S. *J. Chem. Phys.* **2000**, *113*, 2385–2396.
(22) Decornez, H.; Hammes-Schiffer, S. *J. Phys. Chem. A.* **2000**, *104*, 9370–9384.
(23) Pressé, S.; Silbey, R. *J. Chem. Phys.* **2006**, *124*, 164504–164511.
(24) Galoppini, E.; Fox, M. A. *J. Am. Chem. Soc.* **1996**, *118*, 2299–2300.
(25) Suydam, I. T.; Snow, C. D.; Pande, V. S.; Boxer, S. G. *Science* **2006**, *313*, 200–204.
(26) Steffen, M. A.; Kaiqin, L.; Boxer, S. G. *Science* **1994**, *264*, 810–816.
(27) Shin, Y.-G. K.; Newton, M. D.; Isied, S. S. *J. Am. Chem. Soc.* **2003**, *125*, 3722–3732.

10.1021/ja809777j CCC: $40.75

Scheme 1

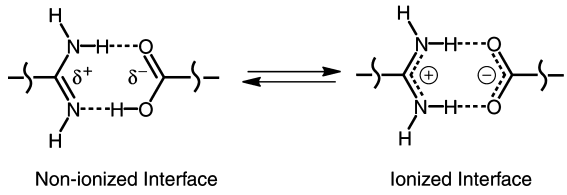

been isolated because of the inability to perform comparative PCET rate measurements on homologous systems featuring ionized versus nonionized proton interfaces.

The two-point hydrogen bond between amidine and carboxylic acid gives rise to the possibility of two proton-interface configurations: a nonionized amidine−carboxylic acid interface and an ionized amidinium−carboxylate interface, both of which are shown in Scheme 1. The proton configuration within the interface has been determined by using a highly conjugated amidinium-appended porphyrin, whose absorption spectrum exhibits distinctive shifts depending on the protonation state of the amidine functionality.[31] A systematic study of a series of binding moieties has shown that the equilibrium configuration of the proton within the interface depends on a balance between the pK_a of the bound acid and the electrostatic energy engendered by the dipole interface.[32] For the case of a sulfonic acid, the pK_a difference is sufficiently large that the ionized amidinium−sulfonate tautomer is preferred in organic solvents of relatively low dielectric constant. Conversely, carboxylic acids yield the neutral amidine−carboxylic acid configuration under the same conditions. With the different tautomeric configurations established, the effect of the proton-interface configuration on PCET can be examined. We now report the comparative PCET kinetics for a Zn(II) porphyrin photodonor (**1**) appended with an amidinium moiety juxtaposed to a naphthalene diimide acceptor functionalized with a carboxylate (**3**) or sulfonate (**4**) functionality; the corresponding dyads **1:3** and **1:4** are depicted in Scheme 2. The work reported herein augments previous PCET and isotope kinetics measurements on **1**:**3**.[8,9] With the rate measurements on **1:4** undertaken, the effects of interface architecture and configuration on the PCET dynamics could be considered and analyzed. We show that the local solvent environment has a large impact on the PCET kinetics of assemblies of identical D−A pairs having different proton configurations within the interface.

Experimental Section

Materials. Silica gel 60 (70−230 and 230−400 mesh, Merck) and Merck 60 F254 silica gel (precoated sheets, 0.2 mm thick) were used for column and analytical thin-layer chromatography, respectively. Solvents for synthesis were of reagent grade or better and were dried according to standard methods.[33] Spectroscopic experiments employed spectroscopic grade tetrahydrofuran (THF), which was dried using standard methods and stored under vacuum. Deuteration of the interface to form **1-D** from **1-H** (the protonated amidinium interface) was accomplished by addition of D_2O from individual ampules (Cambridge Isotope Laboratories). Preparation of **1-H**[34] and naphthalene diimide−carboxylate **3**[8] have been reported previously. Mass spectral analyses were performed at the MIT Department of Chemistry Instrumentation Facility (DCIF) or at the University of Illinois Mass Spectrometry Laboratory.

Physical Measurements. ^{1}H NMR spectra were recorded at 25 °C in the MIT DCIF on a Varian XL-500, Unity 300, or Mercury 300 spectrometer. All chemical shifts are reported using the standard δ notation in parts per million; positive chemical shifts are to higher frequency from the given reference. Absorption spectra were obtained using a Spectral Instruments 440 Series spectrophotometer. Steady-state emission spectra were recorded on an automated Photon Technology International QM 4 fluorimeter equipped with a 150 W Xe arc lamp and a Hamamatsu R928 photomultiplier tube.

Electrochemical experiments were carried out using a Bioanalytical Systems model CV-50W potentiostat/galvanostat. Cyclic voltammetry and differential pulse voltammetry were performed in a two-compartment cell using a glassy carbon disk as the working electrode, a Ag/AgCl reference electrode, and a platinum wire auxiliary electrode. The supporting electrolyte used for electrochemistry experiments was either 0.1 M *n*-tetrabutylammonium hexafluorophosphate ($TBAPF_6$) or perchlorate (TBAP). The solution in the working compartment of the cell was deaerated using nitrogen. Background cyclic voltammograms of the electrolyte solution were recorded prior to addition of the solid sample. Redox couples were referenced to SCE by using a ferrocenium/ferrocene internal standard (0.307 V vs SCE).[35]

The excitation source for transient absorption (TA) and luminescence lifetime measurements was a chirped-pulse amplified Ti:sapphire laser system that has been described elsewhere.[8] In this experiment, the 100 fs, 800 nm output of the regenerative amplifier was frequency-upconverted in a visible optical parametric amplifier (BMI Alpha-1000) to produce a 1 kHz pulse train of excitation pulses at 560 nm for resonant excitation of the Q-band of **1**. The excitation was vertically polarized and attenuated to 50−250 nJ/pulse.

TA spectroscopy was performed on samples contained in a high-vacuum cell comprising a 1-cm path length clear fused-quartz cuvette (Starna cells) connected to a 10 cm^3 solvent reservoir via a graded seal. High-vacuum Teflon valves were used to seal the cell from the environment and the cuvette from the solvent reservoir. The TA spectrum of **1-H**:**3** has been reported previously;[8] single-wavelength TA spectroscopy for **1-H**:**4** is reported here. One aliquot of **1** (1×10^{-7} mol) was added to the cuvette, and a 2 equiv aliquot of **4** (2×10^{-7} mol) was added to the solvent reservoir. The cell was evacuated under high vacuum (10^{-5} Torr) to remove the transferring solvent and leave the two compounds in their separated compartments. Dry THF (0.5 mL) was added to the solvent reservoir by high-vacuum transfer, and the solvent was subjected to three freeze−pump−thaw cycles. The cell was sealed from the environment and removed from the high-vacuum manifold. Single-wavelength TA experiments were first performed on unbound **1-H** under vacuum using resonant excitation of the Q-band of **1** at 560 nm. The isosbestic point ($\lambda_{isosbestic}$ = 654 nm) for the singlet−triplet conversion yield was determined. This wavelength, where the intensity of the TA spectrum was invariant, is the best wavelength for detecting PCET transients.[8] Subsequently, the Teflon stopper between the cuvette and solvent reservoir was opened, and the two compounds were mixed while maintaining vacuum inside the cell, allowing the **1-H**:**4** dyad to be studied.

Single-wavelength TA experiments were performed while mechanically chopping the pump beam at 500 Hz. The probe beam

(28) Seyedsayamdost, M. R.; Yee, C. S.; Reece, S. Y.; Nocera, D. G.; Stubbe, J. *J. Am. Chem. Soc.* **2006**, *128*, 1562–1568.
(29) Seyedsayamdost, M. R.; Reece, S. Y.; Nocera, D. G.; Stubbe, J. *J. Am. Chem. Soc.* **2006**, *128*, 1569–1579.
(30) Sibert, R.; Josowicz, M.; Porcelli, F.; Veglia, G.; Range, K.; Barry, B. A. *J. Am. Chem. Soc.* **2007**, *129*, 4393–4400.
(31) Rosenthal, J.; Hodgkiss, J. M.; Young, E. R.; Nocera, D. G. *J. Am. Chem. Soc.* **2006**, *128*, 10474–10483.
(32) Young, E. R.; Rosenthal, J.; Nocera, D. G. *Chem. Commun.* **2008**, 2322–2324.
(33) Armarego, W. L. F.; Perrin, D. D. *Purification of Laboratory Chemicals*, 4th ed.; Butterworth-Heinmann: Oxford, U.K., 1996.
(34) Yeh, C.-Y.; Miller, S. E.; Carpenter, S. D.; Nocera, D. G. *Inorg. Chem.* **2001**, *40*, 3643–3646.
(35) Bard, A. J.; Faulkner, L. R. *Electrochemical Methods: Fundamentals and Applications*; Wiley: New York, 1980.

Scheme 2

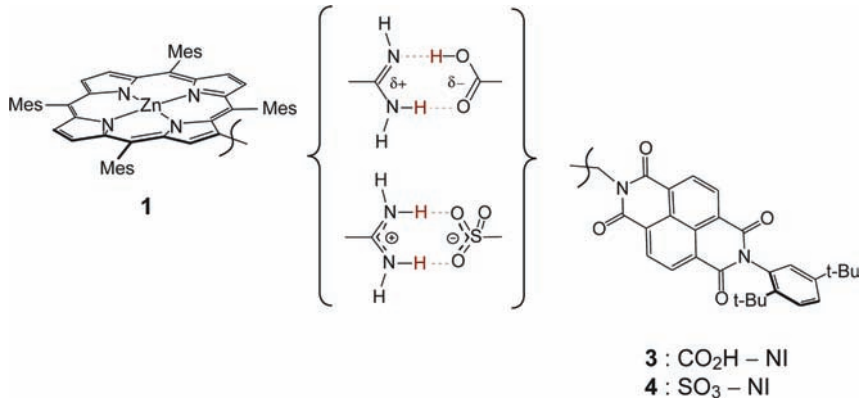

was spectrally resolved in a Jobin-Yvon Triax 320 monochromator, which was used to select a single wavelength (±2 nm) for measurement on an amplified photodiode. The probe beam served as an input signal for a digital lock-in amplifier (Stanford Research Systems SR830) locked at 500 Hz. Data were collected using 10 and 50 ps steps over a range of 3 ns and included some negative time points. The results of twenty forward and backward scans along the stage were collected and averaged.

Samples for variable-temperature experiments were prepared following a detailed procedure outlined previously.[9] To summarize, one aliquot (1×10^{-7} mol) of **1-H** was dissolved in a minimal amount of THF and transferred to a borosilicate short-stem glass ampule (Kimble-Kontes). For deuterium isotopic exchange experiments, a few drops of D_2O were added to the samples prior to the transfer. The samples were sealed from the atmosphere, shaken, and left for 15 min before being transferred to the ampule. The neck of the ampule had been stretched with a flame to reduce the diameter and allow for easier sealing after high-vacuum manipulations. In control or quenching experiments, 4 equiv of benzoate, 4 equiv of **3**, 8 equiv of phenylsulfonate, or 8 equiv of **4** was then added. The ampule containing the sample was attached to a high-vacuum adaptor. The transferring solvents were removed on a high-vacuum manifold ($<10^{-6}$ Torr), and the sample was kept under vacuum for at least 2 h to remove any residual water. Dry THF (1 mL) was added to the ampule by vacuum transfer, and at least three freeze−pump−thaw cycles were performed. The ampule was then flame-sealed while the solvent remained frozen. The high-vacuum manipulations were necessary to ensure that the samples remained free from exposure to the environment or water, which disrupts the hydrogen bonding between the dyads.

Variable-temperature measurements were carried out as described previously.[9] A modular cryogenic refrigeration system (Air Products and Chemicals) consisting of a single-stage helium compressor (model 1RO2A) connected via hoses to an expander module (model DE-202) with a heating element and temperature controller (Scientific Instruments, 9600-5) was interfaced with a custom-made computer program in order to automate the temperature control settings. The expander module was housed within a laboratory interface (model DMX-1) consisting of a vacuum shroud with glass windows for fluorescence spectroscopy in a right-angle configuration and was continuously pumped to maintain a vacuum of $\sim 10^{-4}$ Torr. The ampule containing the sample was mounted on a copper block, and the thermocouple was calibrated at three temperatures: 77 K (liquid nitrogen), 273 K (ice bath), and 293 K (ambient temperature).

Luminescence lifetime kinetics were measured on a Hamamatsu C4334 Streak Scope streak camera that has been described elsewhere.[36] The emission was collected at the magic angle ($\theta_m = 54.7°$) over a 140 nm window centered on the emission peak. A 10 or 20 ns time base was used.

Data acquisition was automated for the variable-temperature experiments. The temperature controller and streak camera were synchronized to enable data collection throughout the entire temperature range. Luminescence measurements were made after a 20 min wait time during which the temperature was adjusted and the sample was allowed to equilibrate. This cycle occurred for each of the temperature data points, which were typically 10−25 K apart. Each sample was cycled through the entire temperature range four times in different sequences to ensure that the data were independent of the sequence.

Temperature-dependent lifetimes of **1-H(D)** alone and bound to benzoate or phenylsulfonate were measured over a temperature range of 120−300 K. Experiments were repeated at least three times with newly prepared samples. Luminescence lifetimes were determined from streak camera data analysis by integrating 15 or 13 nm and 40 or 50 nm slices of the emission peaks centered at 612 and 655 nm for **1**:**3** and **1**:**4**, respectively, and fitting to a monoexponential decay function. Temperature-dependent lifetimes of **1-H(D)**:**3** and **1-H(D)**:**4** were measured at the same temperature points and the data fitted in the same manner, except that the fitting procedure used a biexponential decay function with the longer-lifetime component fixed to the lifetime obtained from the control experiment using **1-H(D)** at each temperature.

Synthesis of Naphthalene Monoanhydride 2. 1,4,5,8-Naphthalenetetracarboxylic acid dianhydride (8.95 g, 33.4 mmol) and 2,5-di-*tert*-butylaniline (3.2 g, 15.6 mmol) were combined in a 250 mL round-bottom flask. To the mixture of reactants was added 75 mL of anhydrous dimethylformamide (DMF). The resulting solution was stirred under an atmosphere of nitrogen and heated at 105 °C for 14 h. After the dark solution was cooled to room temperature, the DMF was removed under reduced pressure. The resulting residue was purified by column chromatography on silica using a solution of 10% ethyl acetate in hexanes as the eluent to remove nonpolar impurities. The desired product was isolated using 1:1 ethyl acetate/hexanes as the eluent to generate 1.34 g of the title compound in 19% yield. ^{1}H NMR (300 MHz, $CDCl_3$): δ 8.84 (s, 4H), 7.62 (dd, J = 8.5 Hz, 1H), 7.53 (dd, J = 8.5, 2.2 Hz, 1H), 7.01 (d, J = 2.2 Hz, 1H), 1.33 (s, 9H), 1.25 (s, 9H).

Synthesis of Naphthalenediimide 4. A solution of monoanhydride **2** (2.0 g, 4.40 mmol) and aminomethanesulfonic acid (3.1 g, 28.0 mmol) in DMF (40 mL) was refluxed under a nitrogen atmosphere for 16 h. The solution was then cooled to room temperature and concentrated under reduced pressure. The crude material was redissolved in CH_2Cl_2 and washed with 5% HCl. The organic layer was then separated, and the aqueous layer was extracted twice with 50 mL of CH_2Cl_2. The organic layers were combined, dried over Na_2SO_4, and reconcentrated under reduced pressure. The resultant residue was chromatographed on silica gel with CH_2Cl_2 to remove nonpolar impurities and then with 75:1

(36) Loh, Z. H.; Miller, S. E.; Chang, C. J.; Carpenter, S. D.; Nocera, D. G. *J. Phys. Chem. A* **2002**, *106*, 11700–11708.

Scheme 3

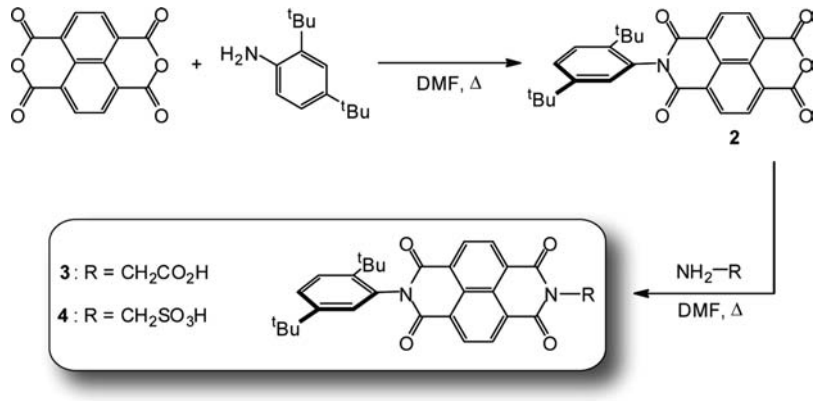

(v/v) CH_2Cl_2/MeOH to furnish the desired product, which was recrystallized from CH_2Cl_2 and hexanes. The purified product was filtered and washed with cold 1:3 (v/v) CH_2Cl_2/hexanes to afford the pure sulfonic acid diimide in 17% yield (0.41 g). ^{1}H NMR (300 MHz, CD_3OD, 25 °C): δ 8.79 (dd, $J_1 = 7.5$ Hz, $J_2 = 7.1$ Hz, 4H), 7.58 (d, $J = 5.3$ Hz, 1H), 7.48 (dd, $J_1 = 3.7$ Hz, $J_2 = 1.5$ Hz, 1H), 7.18 (d, $J = 1.1$ Hz, 1H), 5.42 (s, 2H), 1.31 (s, 9H), 1.23 (s, 9H). ESI-MS $[M - H^+]^-$: calcd for $C_{29}H_{27}N_2O_7S$, *m/z* 547.1539; found, 547.1517.

The sulfonic acid-appended diimide was converted to the corresponding sulfonate salt by dissolving 123 mg (0.240 mmol) of the acceptor in 25 mL of 2% MeOH in CH_2Cl_2 and cooling the resultant solution to −78 °C. In dropwise fashion, 100 μL of tetramethylammonium hydroxide (TMAOH) (25% in MeOH) was added to the cold stirring solution, which was stirred for an additional 5 min at −78 °C and then warmed to room temperature. Concentration of the solution under reduced pressure yielded a solid, which was dried for 14 h under vacuum. A pure product was obtained in quantitative yield. ^{1}H NMR (300 MHz, CD_3OD, 25 °C): δ 8.79 (dd, $J_1 = 7.5$ Hz, $J_2 = 7.1$ Hz, 4H), 7.58 (d, $J = 5.3$ Hz, 1H), 7.48 (dd, $J_1 = 3.7$ Hz, $J_2 = 1.5$ Hz, 1H), 7.18 (d, $J = 1.1$ Hz, 1H), 5.42 (s, 2H), 3.04 (s, 12H), 1.31 (s, 9H), 1.23 (s, 9H). ESI-MS $[M - N(CH_3)_4^+]^-$: calcd for $C_{29}H_{27}N_2O_7S$, *m/z* 547.1539; found, 547.1553.

Results

The supramolecular dyads designed for comparative PCET kinetics investigations, which are displayed in Scheme 2, were formed from association of Zn(II) porphyrin amidinium donor **1** with naphthalene diimide acceptors **3** and **4**. These acceptors were prepared according to the reaction sequence depicted in Scheme 3. 2,5-Di-*tert*-butylaniline was condensed with 1,8:4,5-napthalenedianhydride in refluxing DMF to generate the asymmetric monoanhydride **2**,[37] which was subsequently condensed with glycine or aminomethanesulfonic acid to generate **3** or **4**, respectively. Supramolecular dyads of **1** with these diimide acceptors form well-defined two-point hydrogen bonds possessing favorable primary and secondary electrostatic interactions.[38] A signature of this hydrogen bonding association is the downfield shift of the amidinium protons involved in hydrogen bonding (NH_{ax}) and an insensitivity of the chemical shift of the amidinium protons external to the salt bridge (NH_{eq}). As previously demonstrated for the ^{1}H NMR spectrum of the Ni(II) derivative of the **1:3** dyad in 2-Me-THF,[8] the NH_{ax} protons moved downfield from 10.6 to 12.4 ppm upon their hydrogen-bonding association to the carboxylate ion, whereas the chemical shift of the NH_{eq} protons changed by <0.05 ppm. A similar downfield shift in the ^{1}H NMR spectrum of **1** induced by the addition of **4** (from 10.6 to 12.1 ppm) in THF confirmed that binding in the **1**:**4** dyad occurs through the two-point hydrogen bond (as opposed to axial ligation) of the amidine−sulfonic acid interface. THF binds axially to the Zn(II) porphyrins, thereby preventing porphyrin aggregation caused by axial ligation of the amidine to the Zn(II) porphyrin. Accordingly, the solvent enforces a two-point hydrogen bond as the only structure for dyad assembly.

The equilibrium constant for association of **1** with **3** in 2-Me-THF has previously been determined to be K_{assoc}(**1-H**:**3**) = 2.8 × 10^4 M^{-1} using an analysis of the ratio of pre-exponential factors of the transient emission (TE) decay curves of **1** with varying concentrations of **3**.[9] Because the measurements reported herein were performed in THF, we determined K_{assoc}(**1-H**:**3**) in THF. The static fluorescence quenching from the porphyrin chromophore was monitored upon titration of **1** with **3**. A fit of the emission intensity to the Benesi−Hildebrand equation yielded K_{assoc}(**1-H**:**3**) = 2.4 × 10^4 M^{-1} (THF, 298 K),[8] which closely matches the value derived from the ratio of pre-exponential factors for the bound and unbound lifetimes of **1**.[39] As expected, K_{assoc}(**1-H**:**3**) in 2-Me-THF and THF are similar. With the validity of the lifetime method established, the binding constant of **1-H** to **4** was determined by analysis of the pre-exponential factors of the emission lifetime decay curves to give K_{assoc}(**1-H**:**4**) = 2.9 × 10^2 M^{-1} in THF. The ratio of pre-exponential factors remained similar from 150 to 300 K, indicating that **4** remains bound to **1** throughout the sampled temperature range.

Figure 1 shows the TA kinetics profiles measured at λ = 654 nm for **1** and dyad **1-H**:**4** in THF. Following excitation of the $Q_{1,0}$ band of **1**, a broad TA feature of the porphyrin S_1 excited state is superimposed on bleaching features at 562 and 602 nm that arise from the loss of the ground-state Q-band absorptions. The single-wavelength TA kinetics in this region shows decay profiles arising from intersystem crossing to the T_1 excited state, which can obscure the spectral signatures of the PCET intermediate (porphyrin radical cation, λ_{max} = 412 and 637 nm;[8] diimide radical anion, λ_{max} = 475 and 610 nm[40]). An isosbestic point in the S_1−T_1 TA spectra of unbound **1** provides a dynam-

(37) Iverson, B. L.; Zych, A. J. *J. Am. Chem. Soc.* **2000**, *122*, 8898–8909.
(38) Pranata, J.; Wierschke, S. G.; Jorgensen, W. L. *J. Am. Chem. Soc.* **1991**, *113*, 2810–2819.
(39) $K_{assoc} = Q(Q + 1)/\{[\mathbf{3}]_0(Q + 1) - [\mathbf{1}]_0 Q\}$, where Q is the ratio of the pre-exponential factors of the short (bound) and long (unbound) components, which also corresponds to the ratio [**1**:**3**]/[**1**].
(40) Rogers, J. E.; Kelly, L. A. *J. Am. Chem. Soc.* **1999**, *121*, 3854–3861.

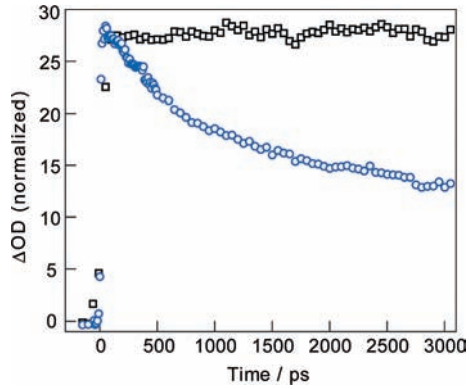

Figure 1. Single-wavelength transient absorption spectra of **1** (black □) and the **1**:**4** dyad (blue ○) at the $S_1 \rightarrow T_1$ isosbestic point of **1**, $\lambda_{obs} = 654$ nm.

ics-free background for single-wavelength observation of the porphyrin radical cation, as previously demonstrated in PCET studies of **1**:**3**.[8] Accordingly, TA was employed in an effort to observe the growth and decay of an optical signature attributed to the porphyrin radical cation in the charge-separated state for the **1**:**4** dyad at $\lambda_{obs} = 654$ nm, the isosbestic point for S_1-T_1 conversion. The dynamics of charge separation in Figure 1 are superimposed on the flat S_1-T_1 absorption profile arising from unbound **1** in solution. On the basis of K_{assoc}(**1**:**4**) in THF (2.9×10^2 M^{-1}), ~25% of the porphyrin is bound by the acceptor at the concentrations used in the TA experiments. The single-wavelength TA kinetics trace for **1**:**4** shows a shoulder with shallow decay instead of a clear growth and subsequent decay as obtained for **1**:**3**. Nevertheless, the TA profile does contain components of (1) formation of the porphyrin radical cation in forward ET followed by (2) depletion of the radical cation via back electron transfer. A biexponential fit to the data was performed by fixing one lifetime component to the forward ET lifetime ($\tau_{em} = 420$ ps), which was obtained by time-resolved fluorescence quenching experiments. This treatment of the data yielded k_{ET}(forward) $= 2.4 \times 10^9$ s^{-1} (298 K) for the growth of the transient signal and k_{ET}(back) $= 3.3 \times 10^9$ s^{-1} (298 K) for the transient signal's disappearance. Details of the kinetics analysis are provided in the Supporting Information (SI). The rate constants for **1**:**4** are significantly greater than the corresponding ones recorded for **1**:**3** [k_{ET}(forward) $= 0.9 \times 10^9$ s^{-1} (2-Me-THF, 298 K), k_{ET}(back) $= 1.4 \times 10^9$ s^{-1} (2-Me-THF, 298 K)]. For **1**:**4**, accumulation of the charge-separated intermediate is not significant because of the faster overall kinetics as well as the fact that k_{ET}(back) > k_{ET}(forward). Kinetic modeling of the TA signatures upon variation of k_{ET}(forward) and k_{ET}(back) was performed, and the results are presented in the SI. At the experimental concentrations employed, for the case in which k_{ET}(back) > k_{ET}(forward), the growth of a charge-transfer intermediate TA signal appears as a shallow rise with subsequent decay (such a feature is observed in Figure 1) instead of a distinct rise and decay as reported previously for **1**:**3**. As discussed in the SI, the shallow rise is a general characteristic of faster ET kinetics with k_{ET}(back) > k_{ET}(forward).

Temperature-dependent rate constants were ascertained from the TE decay kinetics. The fluorescence lifetimes of **1-H** (protonated amidinium) and **1-D** (deuterated amidinium) in THF increased linearly with decreasing temperature (Figure S5 in the SI). Phenylsulfonate (**PS**) binds efficiently to **1** but is not capable of quenching the S_1 excited state of **1** via electron or energy transfer. The **1-H**(**D**):**PS** dyad thus allows the dynamics

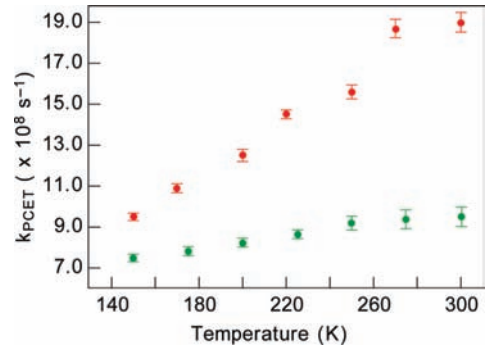

Figure 2. Temperature dependence of the rate of PCET for (green, lower circles) **1-H**:**3** and (red, upper circles) **1-H**:**4** dyads in THF.

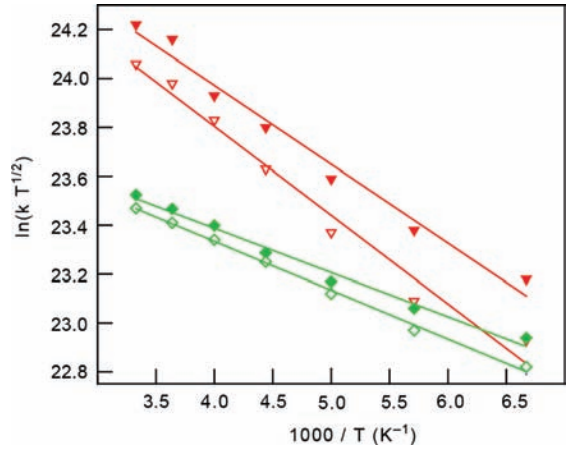

Figure 3. Arrhenius plot depicting the temperature dependence of the PCET rate constants for (a) **1-H**:**3** (green ◆) and **1-D**:**3** (green ◇) in THF and (b) **1-H**:**4** (red ▼) and **1-D**:**4** (red ▽) in THF.

of **1** to be ascertained in the presence of a two-point hydrogen bond but in the absence of excited-state deactivation due to PCET dynamics. The temperature-dependent lifetimes of the **1-H**(**D**):**benzoate** and **1-H**(**D**):**PS** dyads (Figure S6 in the SI) corresponded well with that of **1** alone, and all of the lifetime-versus-temperature plots showed similar slopes, indicating that formation of the two-point hydrogen bond does not affect the excited state dynamics of the Zn(II) porphyrin amidinium species. Conversely, the TE decay profile was dramatically perturbed when the benzoate and **PS** binding moieties were replaced by **3** and **4**, respectively. The fluorescence decays of **1-H**(**D**):**3** and **1-H**(**D**):**4** exhibited a biexponential decay functionality and were fitted with one time constant fixed to the unquenched lifetime of **1-H**(**D**) and the second lifetime varied to obtain the best fit. The lifetime of unbound **1** was independently determined at all temperatures at which PCET measurements were made. The quenched time constant was used to determine the forward rate of PCET using the relation $k_{PCET} = [1/\tau_{\mathbf{1\text{-}H(D)\cdot Q}}] - [1/\tau_{\mathbf{1\text{-}H(D)}}]$, where **Q** = **3** or **4**. Figure 2 plots k_{PCET} values versus temperature for protonated PCET dyads **1**:**3** and **1**:**4** in THF; data for the deuterated dyads was omitted from Figure 2 for clarity but appears in Figure 3, which presents the protonated and deuterated data as Arrhenius plots of the form $\ln(k_{PCET}T^{1/2})$ versus $1/T$ fitted with the semiclassical Marcus formalism. Linear Arrhenius behavior was observed. A distinct kinetic isotope effect (KIE) was seen for each sample, indicating that the photoinduced charge transfer is sensitive to nuclear motions within the intervening proton interface. In the previously reported study of **1-H**(**D**):**3** in 2-Me-THF, the KIE exhibited

disparate behavior with variations in temperature.[9] In the high-temperature regime (300 K), the KIE was $k_H/k_D \approx 1.22(1)$, whereas in the low-temperature regime (120 K), the isotope dependence was inverted to ~0.87(1). As shown in Figure 3, the KIEs for **1-H(D)**:**3** and **1-H(D)**:**4** in THF also exhibited nonparallel behavior over the temperature range studied.

Discussion

The influence that intervening hydrogen bonds exert on the charge-transfer kinetics is revealed when **1**:**3** (Scheme 2) is compared to a closely related system in which the donor and acceptor sites are covalently bound. Introduction of hydrogen bonds between the D and A moieties retards the ET rate by over 2 orders of magnitude. This effect is primarily ascribed to attenuation of the electronic coupling constant, $|V|$. The previously reported value of $|V|$ (~2 cm^{-1}) determined for **1**:**3** is 10-fold smaller than that inferred for covalently bound analogues.[9,41−44] This observation is reaffirmed by the $|V|$ values of ~4 to 12 cm^{-1} for other hydrogen-bonded D···[H^+]···A architectures involving three-point hydrogen-bonded Watson−Crick base pairs.[41−46] Whereas it is clear that hydrogen bonds in D···[H^+]···A systems attenuate the charge-transfer kinetics and D−A coupling, it is not apparent how the internal structure of the two-point hydrogen-bonded interface perturbs the parameters that control PCET. To determine these effects, solvent- and temperature-dependence studies on the **1**:**3** and **1**:**4** dyads were undertaken.

Comparison of the PCET kinetics for **1**:**3** and **1**:**4** enabled an analysis of the charge transfer as mediated by differing proton configurations within a hydrogen-bonded interface. Previous work involving an amidinium-appended purpurin chromophore allows the assignment of the proton-interface configuration in dyads **1**:**3** and **1**:**4**. The amidinium-appended purpurin was titrated with a series of carboxylate and sulfonate binding moieties to determine the protonation state of the bound amidinium group within the assembled interfaces. The pH-dependent UV−vis absorption spectrum of the amidinium-appended purpurin revealed the manner in which a balance between the pK_a values of the constituent acids and electrostatic interactions conspire to produce either an ionized or nonionized interface in THF.[31,32] Those results show that in the present case, the **1**:**3** dyads are bridged by a *nonionized amidine−carboxylic acid interface* while the **1**:**4** dyads are catenated by an *ionized amidinium−sulfonate interface*.

The temperature-dependent kinetic data can be analyzed using the semiclassical Marcus equation[47]

$$k_{ET} = \frac{2\pi}{\hbar}|V|^2\sqrt{\frac{1}{4\pi\lambda k_B T}}\exp\left[\frac{(\Delta G^\circ + \lambda)^2}{4\lambda k_B T}\right] \qquad (1)$$

The activation energy (E_a) of the PCET reaction is furnished by the slope of the kinetics results plotted in the Arrhenius form.

Table 1. Thermodynamic and Kinetic Parameters Measured for Dyads **1**:**3** and **1**:**4** in THF

dyad	solvent	ΔG° (eV)[a,b]	E_a(obs) (10^{-2} eV)[b]	λ_s (eV)[b]	$\lvert V\rvert$ (10^{-4} eV [cm^{-1}])[b]	KIE
1-H:**3**	THF	−0.58	1.56(9)	0.80(1)	3.0(2) [2.4(2)]	1.07(1)
1-D:**3**	THF	−0.58	1.72(5)	0.82(1)	3.1(2) [2.5(2)]	
1-H:**4**	THF	−0.59	2.8(2)	0.91(4)	5.6(9) [4.5(8)]	1.22(2)
1-D:**4**	THF	−0.59	3.1(2)	0.93(4)	5.6(9) [4.5(8)]	

[a] Calculated using the expression $\Delta G^\circ = E_D^{ox} - E_A^{red} - E_{ex} + \Delta G(\epsilon)$, where E_D^{ox} is the oxidation potential of the donor, **1**, E_A^{red} is the reduction potential of the acceptor, **3** or **4**, E_{ex} is the excited-state energy of **1**, and $\Delta G(\epsilon)$ is the solvent-dependent Coulombic term. $\Delta G(\epsilon)$ was calculated using the Born equation with a solvent dielectric constant (ε) of 7.52 (295 K), a D−A distance of 13 Å, and ionic radii of 5 and 4 Å for **1** and **3/4**, yielding $\Delta G(\epsilon) = -0.12$ eV. [b] Obtained from fits to the semiclassical Marcus equation, assuming that ΔG° is temperature-independent.

The calculated E_a values summarized in Table 1 are small relative to the PCET driving force (ΔG°), which is known for each system (Table 1). The total reorganization energies (λ) were determined from the slope of the linear Arrhenius fit as described previously.[9] The λ values range from 0.80 to 0.93 eV for **1-H(D)**:**3** and **1-H(D)**:**4** in THF and match well with a calculated reorganization energy comprising an outer-sphere reorganization energy (λ_o) of ~0.8 eV (based on a D−A distance of 13 Å and ionic radii of 5 and 4 Å for the donor **1** and naphthalene diimide acceptors **3** and **4**, respectively) and an inner-sphere solvent reorganization contribution (λ_i) of ~0.2−0.3 eV for Zn(II) porphyrin donor−diimide acceptor systems.[48,49] With ΔG° and λ determined, the electronic-coupling matrix element $|V|$ was evaluated from the *y*-intercept of the linear fit to eq 1, as has been reported previously.[9] The values of $|V|$ listed in Table 1 ($|V| \approx 1.9-4.5$ cm^{-1}) are smaller than the corresponding values determined for covalently bound systems of similar architectural design and molecular topology ($|V| \gtrsim 10$ cm^{-1}).[48,49]

Comparison of the PCET dynamics and parameters for **1**:**3** and **1**:**4** underscores the sensitivity of charge transfer through hydrogen bonds to the surrounding environment and highlights the effects that are imposed by structural changes within the proton interface. Both **1**:**3** and **1**:**4** maintain a specific asymmetric two-point hydrogen-bonded interface joined via N···H···O hydrogen bonding that mediates the charge transfer between the Zn(II) porphyrin and naphthalene diimide. The driving force for ET varies by only 0.03 eV among the **1-H(D)**:**3** and **1-H(D)**:**4** dyads, which precludes the attribution of the observed changes in PCET behavior to a simple driving-force effect. The nature of the static configuration (nonionized or ionized) of the protonic interfaces in **1**:**3** and **1**:**4** and the difference in the coupling through the sp^2-hybridized carboxylate carbon atom versus the sp^3-hybridized sulfonate sulfur atom emerge as two prominent factors that likely modulate the observed solvent- and temperature-dependent behavior of PCET in these systems. The difference in the electronic coupling through the interface is one manifestation of the PCET. In the case of **1**:**4**, the electronic coupling is through an ionized amidinium−sulfonate interface. Presumably, the Coulombic charge of the ionized interface translates to a shorter distance and stronger coupling for **1**:**4**. Moreover, the internal charge of the ionized amidinium−sulfonate interface of **1**:**4** induces a preorganized solvent structure about the proton interface, leading to stronger coupling

(41) Osuka, A.; Yoneshima, R.; Shiratori, H.; Okada, S.; Taniguchi, S.; Mataga, N. *Chem. Commun.* **1998**, 1567–1568.
(42) Harrison, R. J.; Pearce, B.; Beddard, G. S.; Cowan, J. A.; Sanders, J. K. M. *Chem. Phys.* **1987**, *116*, 429–448.
(43) Davis, W. B.; Ratner, M. A.; Wasielewski, M. R. *J. Am. Chem. Soc.* **2001**, *123*, 7877–7886.
(44) Winters, M. U.; Pettersson, K.; Martensson, J.; Albinsson, B. *Chem.—Eur. J.* **2005**, *11*, 562–573.
(45) Sessler, J. L.; Wang, B.; Harriman, A. *J. Am. Chem. Soc.* **1993**, *115*, 10418–10419.
(46) Sessler, J. L.; Sathiosatham, M.; Brown, C. T.; Rhodes, T. A.; Wiederrecht, G. *J. Am. Chem. Soc.* **2001**, *123*, 3655–3660.
(47) Marcus, R. A.; Sutin, N. *Biochem. Biophys. Acta* **1985**, *811*, 265–322.
(48) Archer, M. D.; Gadzekpo, V. P. Y.; Bolton, J. R.; Schmidt, J. A.; Weedon, A. C. *J. Chem. Soc., Faraday Trans. 2* **1986**, *82*, 2305–2313.
(49) Gaines, G. L., III; O'Neil, M. P.; Svec, W. A.; Niemczyk, M. P.; Wasielewski, M. R. *J. Am. Chem. Soc.* **1991**, *113*, 719–721.

of the reactants to the solvent. This greater solvent coupling is reflected in a larger reorganization energy in **1**:**4** than in **1**:**3**. This larger Franck−Condon term is offset by greater electronic coupling, thus leading to an overall enhancement in the PCET rate constant for **1**:**4**. Thus, PCET finds its origins in both components of the charge transfer, namely, the electronic-coupling and Franck−Condon terms.

Modulation of the coupling to the solvent is revealed by the KIE. It should be noted that the lines in the Arrhenius plots in the KIE studies (Figure 3) are nonparallel. This temperature-dependent behavior of PCET rates can lead to a crossover in the KIE.[9,50] This unusual phenomenon has been attributed to the freezing out of hydrogen vibrational modes within the interface as the temperature decreases. Fluctuations within the hydrogen-bonded bridge dynamically modulate the electronic coupling for ET, and consequently, the rate of charge separation becomes sensitive to the nature of the proton modes within the bridge. The nonparallel slopes in the KIE data for **1**:**3** and **1**:**4** in THF lead to ∼7 and ∼9% increases in the respective KIEs over the temperature range sampled. This KIE trend is in contrast to the KIE data previously reported for **1**:**3** in 2-Me-THF, which yielded a decrease in KIE of ∼18% over a similar temperature range.[9] The KIE trend for **1**:**3** and **1**:**4** in THF is typical of predictions made by conventional PCET theory.[22,51] The molecular differences between solvents used in these two studies may be a contributing factor in dictating the temperature-dependent behavior and are the focus of continuing research efforts.

In summary, a direct comparison of PCET is facilitated by the similarity of the **1**:**3** and **1**:**4** PCET systems, which accentuates the differences introduced by the two proton interfaces. The importance of the proton interface is revealed by the different values of λ_s, E_a, and $|V|$ for **1**:**3** and **1**:**4**. Stronger coupling of the PCET reaction is observed for interfaces that are ionized. Efforts to measure this solvent coupling directly by two-dimensional methods are currently underway.

Acknowledgment. J.R. thanks the Fannie and John Hertz Foundation for a predoctoral fellowship. This work was supported by the National Institutes of Health (GM 47274).

Supporting Information Available: Fitting and kinetic modeling of transient absorption data; additional variable-temperature data for **1**, **1**:**benzoate**, and **1**:**PS**. This material is available free of charge via the Internet at http://pubs.acs.org.

JA809777J

(50) Cape, J. L.; Bowman, M. K.; Kramer, D. M. *J. Am. Chem. Soc.* **2005**, *127*, 4208–4215.

(51) Hammes-Schiffer, S.; Hatcher, E.; Ishikita, H.; Skone, J. H.; Soudackov, A. V. *Coord. Chem. Rev.* **2008**, *252*, 384–394.